DAShip: A Large-Scale Annotated Dataset for Ship Detection using Distributed Acoustic Sensing Technique

Wenjin Huang, Shaoyi Chen, Yichang Wu, Ruihua Li, Tianrui Li, Yihua Huang*, Xiaochun Cao*, and Zhaohui Li*

***Abstract*—Ship detection and identification is the key part of the maritime monitoring and safety. Ship monitoring methods based on coastal video surveillance, satellite imagery, and synthetic aperture radar have been well developed. As the emerging remote sensing technology, distributed acoustic sensing (DAS) technology which continuously detects vibrations along underwater optical fiber cables facilitates all-weather, all-day, and real-time ship detection capabilities, possessing the potential for detecting dark ships. However, the reliance on expert knowledge for analyzing ship passage signals hinders the development of an automated framework for ship detection, limiting the application of DAS technology in the ship detection. Additionally, the scarcity of datasets for ship passage events in the DAS field hampers the adoption of deep learning technologies for enhancing ship detection. To address these challenges, an automatic annotation method is proposed, utilizing 18625 cleaned ship records based on the automatic identification system to annotate ship passages adaptively from 5-month DAS data. Thus a large-scale, high-quality annotated dataset named DAShip is established, containing 55875 ship passage samples. Furthermore, an online ship detection and identification framework is proposed to achieve real-time ship detection from the massive DAS data flow and further identify coarse-grained ship features, such as ship speed, heading, angle, and ship type. In this proposed framework, YOLO models, primarily trained on DAShip, are used as ship detectors and ship feature classifiers, achieving accurate dark ship detection combined with automatic identification system message and demonstrating competitive performance in ship feature classification.**

***Index Terms*—Dataset, dark ship, distributed acoustic sensing.**

I. Introduction

SHIP detection plays a crucial role in the maritime domain, especially in ensuring navigational safety and conducting traffic flow statistics. However, Automatic Identification System (AIS) that requires ships to actively report their positions confronts challenges including AIS switch-off, spoofing, and tampering, which undermine the accuracy of ship monitoring. Therefore, integrating AIS with other monitoring methods to detect the ships that do not transmit or transmit fake AIS information (dark ships) attracts increasing attentions [1], [2].

Researchers have investigated various technologies for active ship monitoring, including Synthetic Aperture Radar (SAR), satellite imaging and video surveillance. To take advantage of deep learning model, the high-quality datasets have been developed, such as High-Resolution SAR Imagery Dataset (HRSID) [3], a multi-scale ship dataset (OSSD) [4], DOTA [5] and HRRSD [6], SeaShips [7], and SWIM [8].

However, SAR images are vulnerable to interference from complex background clutter, and the features of small ships are often of low significance, further obscured by motion blur [9], making it easy to be obscured by the clutters. The quality of images captured through aerial photography and video surveillance methods is frequently compromised by external environmental factors such as lighting conditions, weather, and cloud cover. Therefore, this paper will employ an emerging vibration sensing technology for ship detection, which is not influenced by external environmental factors such as weather and lighting, and can serve as an effective complement to the aforementioned detection methods.

Distributed Acoustic Sensing (DAS) detects changes in backscattered light caused by acoustic waves along the entire length of fiber optic cables, offering real-time, long-range, high-sensitivity, and all-weather vibration monitoring. By utilizing submarine optical fiber cables, the ship detection system based on DAS provides a unique visual representation of ship wakes in the form of spatial-temporal vibration images, as opposed to the optical top-down images of ships provided by SAR. This approach enhances resilience against cloud cover and adverse weather conditions.

Studies have successfully detected ship movement signals using the DAS technique [10]–[13], underscoring the potential of DAS in ship detection. However, these studies often rely on AIS information to locate the ship passage event within vast DAS data, and then analyze the ship's geolocation by fitting the frequency shift curves in Doppler analysis and leveraging beamforming technique, which complicates the implementation of automated ship detection systems.

Wenjin Huang, Shaoyi Chen, Yichang Wu,Ruihua Li and Tianrui Li are with the School of Electronics and Information Technology, Sun Yat-sen University, Guangzhou 510006, China.

Corresponding author: Yihua Huang is with the School of Electronics and Information Technology, Sun Yat-sen University, Guangzhou 510006, China, and also with Southern Marine Science and Engineering Guangdong Laboratory, Zhuhai 519080, China (e-mail: huangyih@mail.sysu.edu.cn).

Corresponding author: Xiaochun Cao is with School of Cyber Science and Technology, Shenzhen Campus, Sun Yat-sen University, Shenzhen 518107, China. E-mail: caoxiaochun@mail.sysu.edu.cn.

Corresponding author: Zhaohui Li is with the Guangdong Provincial Key Laboratory of Optoelectronic Information Processing Chips and Systems, School of Electrical and Information Technology, Sun Yat-Sen University, Guangzhou 510275, China, with the Key Laboratory of Optoelectronic Materials and Technologies, Sun Yat-Sen University, Guangzhou 510275, China, and also with the Southern Marine Science and Engineering Guangdong Laboratory (Zhuhai), Zhuhai 519000, China (e-mail: lzhh88@mail.sysu.edu.cn)

Manuscript received April 19, 2021; revised August 16, 2021.

Generally, these expert-based ship detection methods are unable to meet the requirements for timely detection of ship passage events within massive DAS data in complex environments, while deep learning technology provides an effective solution for online and automated ship passage detection. However, the images of ship vibration signals in DAS data differ substantially from existing natural image datasets such as ImageNet or COCO, necessitating a dedicated dataset specific to DAS-based ship vibration signals. To the best of our knowledge, there remains a scarcity of DAS-based ship datasets, which poses challenges in applying deep learning techniques for dark ship detection. Therefore, a large-scale, high-quality dataset of ship passages for DAS is required.

To construct the dataset, two key challenges must be addressed. Firstly, the continuously collected DAS data is so vast. Due to the high sample rate and high spatial resolution, the DAS data volume of an 8-km cable reaches up to 20 TB, posing a significant challenge for manual annotation of large-scale ship passage events. Secondly, for slower-moving vessels, the vibration signals are more likely to be obscured by wave noise, affecting the quality of annotation of ship passage in DAS data.

Hence, this paper employs AIS-based ship records to automate the identification of ship passage signals within the extensive DAS data, providing a foundation for the construction of large-scale datasets. But the raw AIS records faced with issues such as timestamp precision errors and data loss [14], and thus this paper first employs a cleaning process for the AIS data to enhance the precision of ship passage trajectory estimation, facilitating the more precise localization of large-scale ship passage events within the DAS data.

In the location process, the slower-moving vessels not only exhibit signals with a lower signal-to-noise ratio but also pose greater difficulties in AIS-based positioning because the longer intervals between AIS data transmissions make it more challenging to infer accurate AIS-based ship trajectories. Therefore, to address the challenges, this paper proposes an adaptive annotation approach to enhance the coverage and accuracy of annotating slower-moving ship passage events, thereby further improving the quality of the dataset.

Furthermore, in the ship detection applications, wave signals constitute the background in DAS-based data, as vessel traffic is not continuously present. Therefore, an environmental wave dataset (Waveset), excluding any ship passage events, is also developed. The Waveset provides abundant negative samples, enabling the trained model to differentiate between background signals, aiming to reduce the false positive rate of the ship detection system.

To evaluate the aforementioned dataset, this paper initially trains network models such as YOLO and Faster R-CNN to develop a ship passage detector, achieving promising results.

Furthermore, this paper proposes an online and real-time ship detection and identification framework, to facilitate dark ship detection and coarse-grained ship feature identification, encompassing attributes such as ship speed, heading, angle, and ship type. Specifically, the real-time DAS data flow entering this framework is segmented according to the sample image size of DAShip and then processed by the detector to obtain potential ship events, which are subsequently compared with AIS records to detect dark ships. The detected ship images are further analyzed by a trained classifier to determine the coarse-grained attributes of speed, heading, angle, and ship type. This two-stage ship identification process, involving detection followed by classification, effectively reduces the overall computational complexity, thereby enhancing real-time performance.

Finally, by processing the continuous 8-days DAS data that was not used in the datasets construction, the framework successfully detects most of ships reported in AIS along with two unreported dark ships.

The main contributions of this paper are:

(1) Utilizing the proposed AIS processing method and adaptive annotation approach for slow-moving ships, a large-scale and high-quality annotated dataset for ship passage events based on DAS data (DAShip) is constructed, comprising 55875 images, 18625 ship instances with detailed annotations of ship speed, heading, cross angle, and ship type. Additionally, a Waveset comprising 93633 images devoid of ship passage events is introduced to provide abundant negative samples, enhancing the ship detector's capability to differentiate background signals.

(2) To achieve dark ship detection, a two-stage ship detection and identification framework for real-time DAS data flow is proposed. In the ship detection stage, this framework uses a spatial and time overlapped method to increase the ship detection robustness and provide an overlapped ship detection method to generate a more accurate ship passage event. In the ship identification stage, only the image containing potential ship passage events is processed to effectively reduce the overall computational complexity. Subsequently, a continuous 8-days DAS data flow is processed, successfully identifying dark ships.

II. Related work

A. Existing ship detection methods

Synthetic Aperture Radar (SAR) technology enables long-distance surveillance by emitting electromagnetic pulses and capturing their reflections from objects. The High-Resolution SAR Imagery Dataset (HRSID) offers a large number of high-resolution SAR images for ship detection, semantic segmentation, and instance segmentation tasks [3]. The HRSID includes SAR images with diverse resolutions, polarizations, sea conditions, maritime areas, and coastal ports, encompassing a total of 5604 high-resolution SAR images and 16951 ship instances.

Due to the imaging principle, SAR images often encounter challenges such as speckle noise, nearshore interference, multi-scale targets, complex backgrounds, and ship motion blur [9]. Small vessels, in particular, pose detection difficulties due to their weak scattering and blurred contours. Enhancing small vessel feature extraction boosts ship detection model performance. Zhou et al. [15] tackle SAR imaging's side-lobe effect with dual-pooling. Zhu et al. [16] introduce a multi-scale detection method for SAR images, addressing high-level feature map issues and imbalance. Hu et al. [17] enhance small ship detection by fusing feature maps with dynamic

sparse attention. Liu et al. [4] create the OSSD dataset and an improved YOLOV5 for small ship detection across various backgrounds and scales.

In the ship monitoring using the satellite or aircraft imaging, DOTA [5] and HRRSD [6] are commonly employed, comprising 2806 and 21761 annotated aerial images, respectively. These datasets include a variety of categories, including ships, as well as other objects such as bridges, cars, and airplanes, with a primary focus on annotating ship hulls. However, Xue et al. argue that, due to constraints imposed by the complex terrain of ports or the resolution of the collected data, vessel wakes are more suitable for detection than hulls, as wakes present more distinctive features in imagery. They first developed a large-scale vessel wake image dataset named SWIM, which includes data samples from visible-band satellites and airborne imaging, comprising 15356 wake annotation instances [8].

Additionally, video surveillance technology is widely used in ship monitoring applications. The installation of cameras in critical waterways and ports allows for the real-time monitoring of ship movements, facilitating the identification of anomalous sailing occurrences. The SeaShips [7] have annotated ships in images and videos, comprising 31455 annotated ship instances at a resolution of 1920×1080. The annotated ships are primarily classified into six categories: ore carriers, bulk cargo carriers, general cargo ships, container ships, fishing boats, and passenger ships.

Gaining further information such as ship speed, heading, and length can help distinguish the motion status of ships. Kang et al. [18] have developed a technique for wake detection and speed estimation by analyzing the distance from a ship's stern to the wake's vertex in SAR imagery, leveraging the relationship between the Doppler effect and radial velocity. Joshi et al. [19] introduced an eigenvalue decomposition (EVD)-based approach for estimating ship size and heading. This method involves computing the covariance matrix from the ship's pixel coordinates and applying EVD to identify the principal and minor axes of the elliptical shape, thus deriving the ship's length, width, and orientation.

The significance of developing real-time data processing and analytics frameworks is underscored by work [20]. Consequently, researchers account for the computational complexity of algorithms to guarantee real-time functionality in practical scenarios. Zhang et al. [21] have introduced a lightweight ship detection module that filters out the majority of sea and coastal backgrounds, focusing processing on potential ship-containing regions to optimize the model's computational burden. Additionally, to achieve a balance between performance and computational burden, researchers have developed lightweight detection models such as LFer-Net [22], HFFANet [23], and ShipDetectionNet [24].

B. DAS methods

The DAS technology has been widely applied in various fields, including pipeline leakage detection [25], [26] and intrusion detection [27], [28], particularly in Vertical Seismic Profiling(VSP). To improve the Signal-to-Noise Ratio of VSP signals, Yue Li et al. propose a series of deep learning models, such as MPFAN [29], MSDN [30], SPSNet [31], DuGAN [32], and Urefiner [33] to remove complex noise from DAS VSP data and recover the underlying valid signals. Additionally, Lv et al. [34] have achieved the detection of seismic signals from vast amounts of DAS data using limited seismic samples, highlighting the ongoing challenge of dataset scarcity in the field of seismic monitoring. Min et al. [35] explore the potential of utilizing DAS and machine learning technologies to identify and extract vehicle signals for urban traffic monitoring.

Existing studies [10]–[13] have demonstrated the effectiveness of DAS for detecting ships near optical fiber cables. Researchers have utilized Doppler shift analysis in acoustic signatures to calculate ship speeds and employed beamforming techniques for localization. DAS has also exhibited sufficient sensitivity to detect small vessels, as evidenced by its capability to detect signals from passenger ships at distances of up to 200 meters from submarine cables [13]. Furthermore, DAS has been successfully applied for ship localization in noisy shallow waters, even with suboptimal cable coupling to soft sediments [36]. These results underscore the promising potential of DAS in the field of ship detection.

However, in shallow water, the faint vibration (including ship wakes and engine sounds) can be overwhelmed by wave signals, posing difficulties in extracting ship passage signals from the massive raw DAS data. The AIS-based ship passage records are used to precisely locate ship vibration signals within the vast DAS data. In the analysis process of work [13], a data window of 10 ms and a channel window of 140 were used, accounting for approximately 0.002% of the total DAS data volume per minute. However, the methods that rely on AIS-based ship records to locate ship vibration signals are not suitable for dark ship monitoring scenarios. Moreover, the analysis of ship positions in these methods requires specialized expertise, such as fitting frequency shift curves in Doppler analysis, which complicates the development of automated ship detection systems.

III. Background

In this paper, Silixa's Distributed Acoustic Sensor ($iDAS^{TM}$) is employed to gather strain signals from a submarine optical cable stretching from Guishan Island to Sanjiao Island in Zhuhai, Guangdong, China, as depicted in Fig.1. The water depth is about from 5 meters to 15 meters. The segment of the cable utilized for measuring ship passage events spans approximately 8.5 km. The iDAS device has a data sampling time resolution of 1 kHz and a spatial resolution of 4 meters. The data collecting time is from 2023/11/14 to 2024/03/27.

A. Characteristics of AIS data

An AIS message includes the current dynamic information (position, heading, and speed), static information (length, draught, and breadth), and other voyage-related information about a ship such as Maritime Mobile Service Identity (MMSI) which can identify a ship uniquely. A sequence of continuous AIS messages is presented in Table I. The longitude and

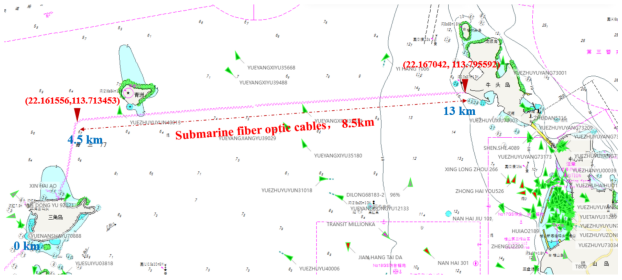

Fig. 1. Submarine Optical Cable Deployment Diagram (https://ais.msa.gov.cn/).

TABLE I
AIS MESSAGE ABOUT THE SHIP(MMSI:413231470[a]), 2021/09/06.

Time	Longitude ($E°$)	Latitude ($N°$)	Velocity (Kn[b])	Ship Type[c]	Length (m)
11:53:42	113.7847	22.1895	31.6	40	40
11:54:00	113.7842	22.1869	31.5	40	40
11:54:14	113.7838	22.1848	31.6	40	40
11:55:09	113.7823	22.176	31.7	40	40
11:55:33	113.7817	22.1734	31.6	40	40

[a] MMSI: Maritime Mobile Service Identity, which is unique to each ship.
[b] $1\ Kn \approx 1.852\ Km/h \approx 0.514\ m/s$ in the South China Sea.
[c] ShipType: GB/T 20068-2017.

latitude coordinate system used in AIS messages is WGS84. The broadcasting interval typically ranges from 2 seconds to 3 minutes, and the faster the ship's speed, the shorter the AIS reporting interval required by regulations.

As aforementioned, beyond the issues of data errors and loss within AIS messages, and the impact of extended reporting intervals on the precision of calculated ship positions, the application of AIS records to pinpoint ship passages in DAS data reveals that the latitude and longitude derived from AIS may not accurately align with the ship's actual position above the optical cable. This discrepancy arises because the reported coordinates reflect the location of the AIS device, not the vibration signals detected by the cable.

In this paper, the maximum spatial distance difference between the AIS-based position and the vibration source of ship is considered as the ship's length. The ship's intrinsic passage time is defined as the ratio of its length to its speed. For ships with low speeds and considerable lengths, their intrinsic passage time can result in significant discrepancies between the AIS-reported position and the position sensed by the cable. This intrinsic passage time is a critical factor that will be incorporated into the proposed adaptive annotation methods.

B. Ship passage event perception

In this paper, the ship wake is utilize as the primary feature in the DAShip and thus the mechanism by which the DAS device measures the ship wakes is discussed as follows. The way in which the ships cross the optical cable influences the pattern of ship passage signal detected by the DAS. At high speeds, ships produce an intensive ship wake on water surface, as depicted in Fig.2. Ship wake theory claims that the wake pattern is mainly determined by the ship speed and the

Fig. 2. Top-down View of the Wave Pattern Created by a High-Speed Vessel on the Water Surface.

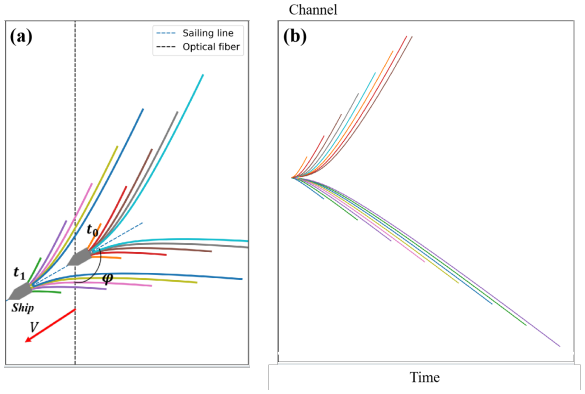

Fig. 3. Principle of Ship Wave Perception by Submarine Optical Cable:(a) Top-down View of Vessel Passage Events; (b) Cross-sectional Pattern of Ship Wave Perception by Submarine Optical Cable.

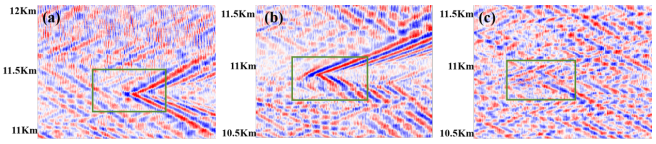

Fig. 4. Signal of Vessel Passage Events Perceived by DAS.

water depth. However, the vibration signal perceived by the submarine optical cable is the cross-section of the ship wake, not the complete wake, as illustrated in Fig.3. Consequently, the ship wake pattern in DAS data is determined by the ship speed, water depth which related to the location of ship passage, and the cross angle(φ) shown in Fig. 3.

The ship passage event depicted in Fig.4(a) occurred on December 29, 2023, at 12:57:29, with the ship traveling at a speed of 16.31 m/s and at an angle of 87.93°, passing over the submarine optical cable at 11.35 km. Fig.4(b) illustrates another ship passage event on February 29, 2024, at 09:16:17, with the ship traveling at a speed of 14.56 m/s and at an angle of 54.36°, passing over the submarine optical cable at 11.00 km. Due to the different cross-angles, the ship wake patterns in Fig.4(a) and (b) differ. In Fig.4, the green boxes include the positions that ships pass over the fiber cable.

When the ship sails at a lower speed, the weak ship wake is often more challenging to detect. Instead, the periodic signals emitted by the ship's engine or propeller can still be perceived. Fig.4(c) illustrates a ship passage event that occurred on March

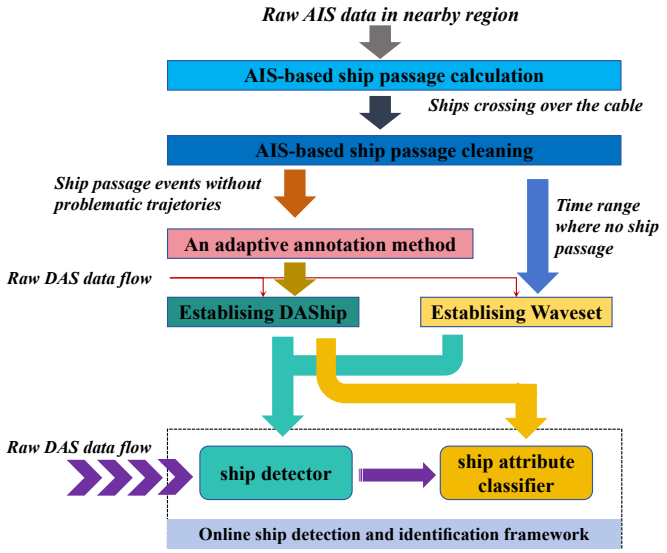

Fig. 5. Overview of dataset construction and the ship detection framework.

26, 2024, at 17:55:19, with the ship traveling at a speed of 2.83 m/s and at an angle of 103.54°, crossing over the submarine optical cable at 10.93 km. The vibration signals perceived by iDAS are depicted in the green box in Fig.4(c). It is evident that the primary pattern of ship passage signals in the DAS data predominantly includes the ship wake and the periodic vibrations of the ship's engine or propeller.

IV. Method

In this section, the construction of DAShip and Waveset are discussed in details. Then, how to use these datasets in the proposed framework is introduced. The relationship of the data construction and the proposed framework is shown in Fig.5.

A. AIS data processing

Algorithm 1 Get AIS-based ship passage events

```
Sort AIS records by ascending Time
Group AIS records by MMSI
for mmsi in MMSI do
    R ← all record[mmsi]
    for r = 0 to len(R)-1 do
        get trajectory(l) from longtitude(lng) and latitude(lat) of R[r] and R[r+1]
        if l cross the submarine optical fiber(L) then
            get CrossPosition (lng_c, lat_c) of l and L
            get CrossTime and CrossSpeed assuming the ship in uniform acceleration motion
        end if
        return mmsi, CrossTime, CrossPosition, CrossSpeed, Angle, Heading, ShipType
    end for
end for
```

TABLE II
SHIP PASSAGE EVENTS.

MMSI	Cross Time	Cross Position (km)	ΔT (minute)	Cross Speed (m/s)	Average Speed (m/s)	$Error\_speed^a$
477856700	2023/11/14 20:32:09	11.73	0.1	6.57	6.506	0.9%
412478605	2023/11/20 12:20:25	5.24	26.02	0.146	0.173	18.4%
412000000	2023/11/17 14:53:51	6.48	0.2	3.45	600.50	17300%

$^a Error\_speed = |Average\ speed - Cross\ speed|/Cross\ speed$

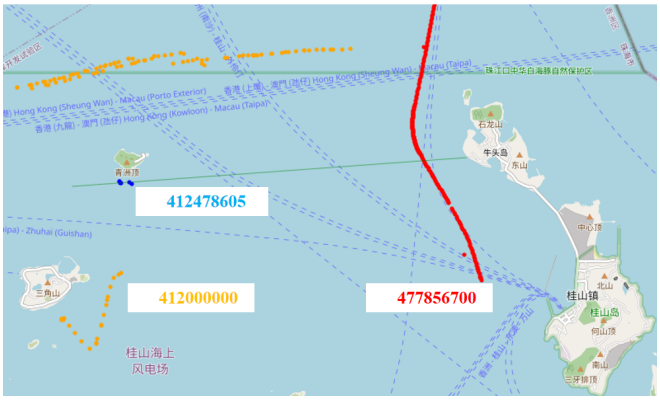

Fig. 6. Ship Passage trajectories.

1) AIS-based ship passage calculation: Taking into account the discrete time intervals between consecutive AIS messages, this paper assumes that ships maintain uniform acceleration motion during these intervals. The calculation of the crossing time and latitude/longitude information of ship passage is outlined in algorithm1.

2) AIS-based ship passage cleaning: After calculating the AIS-based ship passage events, it is necessary to refine these events to remove the problematic events. Specifically, table II illustrates three estimated AIS-based ship passage events, and the corresponding sailing trajectories are depicted in Fig.6 over a 30-minute duration. The ship trajectory with MMSI 412478605 indicates the ship is in a slow-moving state. For the ship with MMSI 412000000, numerous data points exhibit positional drift, leading to a disjointed ship trajectory. To address this issue, latitude and longitude information, as well as time interval information from AIS messages before and after ship passage over optical cables, are utilized to compute the average ship passage speed. This average speed is then compared with the speed reported in AIS messages to calculate the error of speed ($Error\_speed$), which can be used to filter out the trajectory with position drift. Consequently, the ship trajectories with speed differentials less than 30% and AIS message time intervals shorter than 18 seconds are retained, eliminating problematic AIS-based ship trajectories. Additionally, ship events with reported speed of less than 1 m/s are further removed as they are likely drifting or at anchor, thereby eliminating slow-moving ship trajectories.

By using the proposed AIS data processing and cleaning method, 18625 authentic AIS-based ship passage events are obtained. Using the time and position information of these passage events, the samples of DAShip can be generated

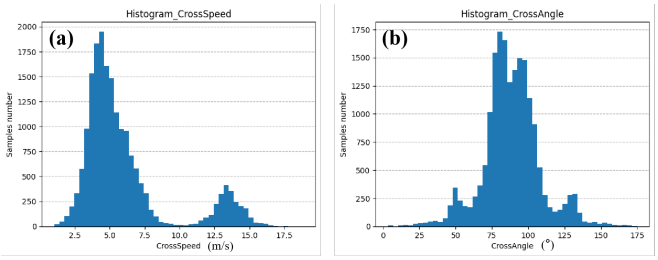

Fig. 7. (a) Ship speed distribution; (b) Ship angle distribution.

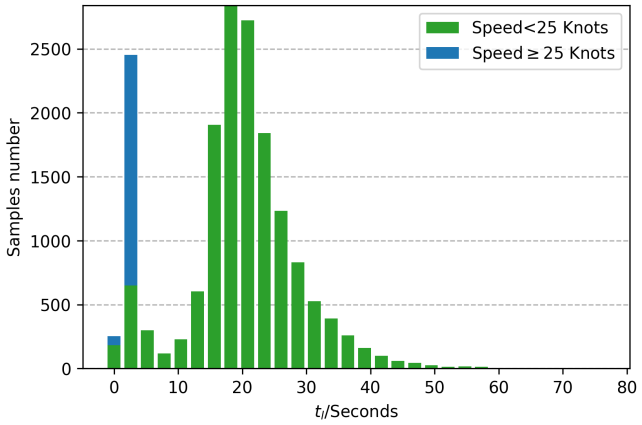

Fig. 8. Distribution of Ship Intrinsic Passage Time of AIS-based Ship Passage Events.

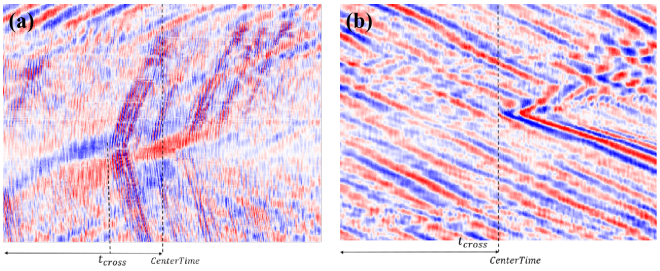

Fig. 9. Illustration of Vessel Passage Time Error:(a) Low-speed Vessel Passage Events; (b) High-speed Vessel Passage Events.

automatically from the vast DAS data.

B. Adaptive annotation method

Among the calculated ship passage events, the distribution of ship speed and ship angle are shown in Fig. 7(a) and (b), respectively. Generally, a ship traveling at a speed greater than 25 knots is usually considered a high-speed ship. Fig.8 illustrates the distribution of intrinsic passage times(t_l) for high-speed and low-speed ships. For high-speed vessels, intrinsic passage times are frequently less than 4s, and the AIS-based cross time tends to more accurately reflects the actual cross time of high-speed ships. However, for low-speed ships, the intrinsic passage times are typically between 15s and 30s, with a maximum of 60s. Consequently, significant time errors may arise when locating low-speed ships in DAS data using the cross time derived from AIS data. Besides, the high-speed ship passage events exhibit more intense signals than low-speed ship passage events, as depicted in Fig.9.

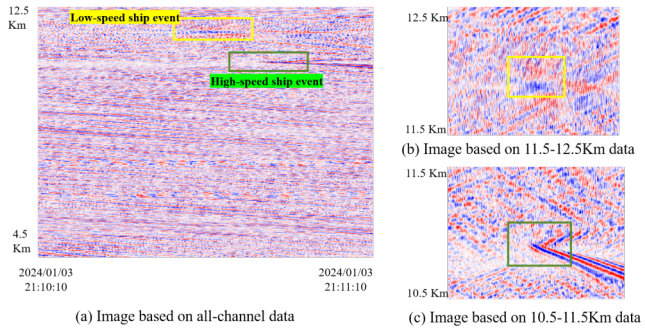

Fig. 10. Texture Details of Samples in Different Spatial Ranges.

Fig.9(a) depicts a ship passage event that occurred on December 4, 2023, at 22:25:26, where a ship with a length of 176 meters traveled at a speed of 7.61 m/s and at an angle of 76.6° over the cable at 11.92 km. Fig.9(b) illustrates another ship passage event that occurred on December 29, 2023, at 10:20:47, where a ship with a length of 55 meters traveled at a speed of 14.35 m/s and at an angle of 124.59° over the cable at 8.54 km.

In Fig. 9, it is apparent that for high-speed ships, the passage time aligns with the $CenterTime$, indicating that $CenterTime$ can accurately annotate the passage time of high-speed ships, while for low-speed ships, the onset of ship passage events in DAS data occurs earlier than the calculated $CenterTime$ based on AIS data. This discrepancy primarily arises from the ship intrinsic passage time. Therefore, an adaptive annotation method based on ship intrinsic passage time is required to improve the accuracy of the low-speed ship passage annotation.

Specifically, the annotation box size for high-speed ships should be minimized to improve the accuracy of locating high-speed ship passage time and position. In the annotated images, the ratios of width and height of the annotation box are set to 0.3, the duration of annotated data is 18 seconds, and the spatial coverage is 0.33 km.

Notably, the size of the annotation box for low-speed ships is determined based on their intrinsic passage time, aiming to encompass as many low-speed ship passage events as possible. For the annotation of low-speed ships, the adaptive width and height ratios of annotation box are determined by $t_l/60$, while the lower and upper limits are set to 0.3 and 0.8. In summary, this annotation method provides a more accurate annotation for high-speed ship and an adaptive annotation box based on ship's intrinsic passage time for low-speed ship, thereby reducing the annotation error.

C. Establishing DAShip

Given the clean AIS data, the DAShip can be established. Using the precise CrossTime and CrossPos, the data of the corresponding ship passage event can be extracted from the massive DAS data. To generate high-quality samples, the following sample settings are introduced.

1) Sample setting: The sensing range of the submarine optical cable ranges from 4.5 km to 12.5 km. In DAShip,

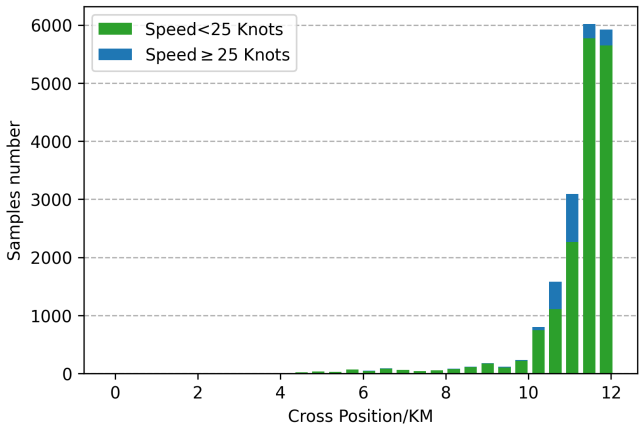

Fig. 11. Distribution of Vessel Passage Locations.

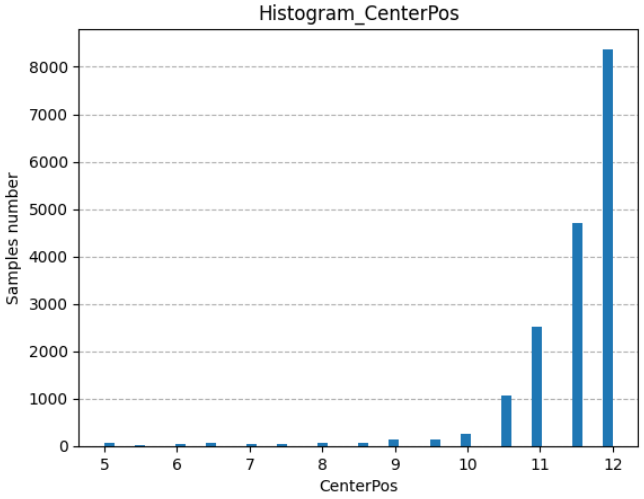

Fig. 12. Distribution of Sample Position Centers.

each sample only includes a segment of the sensing range of fiber cable, with the central positions of the sample images located at 5, 5.5, 6, ..., 12 km along the cable, and each sample comprises the DAS data with 1-minute duration and 1 km spatial segment of optical cable. To reduce the storage overhead of the dataset, the temporal resolution of samples was decreased from the original 1 kHz to 10 Hz.

Initially, segmenting the entire sensing data into multiple samples can enhance texture details at a consistent image size. The texture details under different spatial ranges are shown in Fig.10. The sample images in Fig. 10(a) are constructed from all data within the 4.5 km to 12.5 km range, where the vibration signals of low-speed ship passage events are less pronounced compared to those in Fig. 10(b). Compared to directly constructing samples with all data, the sample constructed with localized data exhibits higher spatial resolution, thereby enhancing the detection effectiveness of low-speed ship passage events.

Furthermore, considering that submarine cables usually extend from several kilometers to a dozen kilometers or more, the approach of using a 1-kilometer data segment as a sample,

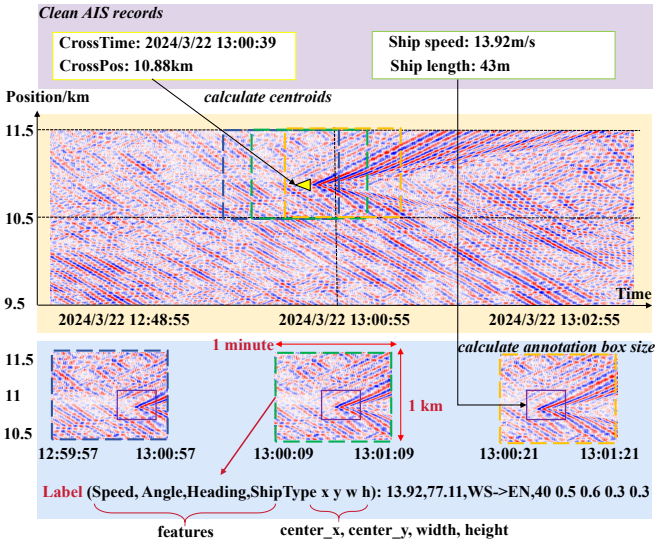

Fig. 13. Details of DAShip construction.

rather than taking the entire 8.5-kilometer length of cable for sampling, evidently enhances the versatility of DAShip for applications with optical cables of varying lengths.

Lastly, unlike using ship passage positions as sample centroids, employing specific locations as sample centroids facilitates the embedding of cable position information into the samples, enabling the mapping of detected ship passage positions to their actual cable positions.

In DAShip, the distribution of ship passage positions and sample centroids is illustrated in Fig.11 and 12. Ship passage positions are predominantly concentrated around the 10-12 km segment of the optical fiber cable, as this area serves as the primary navigational route near Guishan Island.

Algorithm 2 Establishing DAShip

$\Delta T \leftarrow 0.2\ minutes$
$\Delta D \leftarrow 0.5\ km$
$T \leftarrow 1\ minute$
$CenterPos \leftarrow [5, 5.5, 6, ..., 12] km$
E ← AIS-based ship passage events
for *event* in **E** **do**
  $ct \leftarrow event.CrossTime$
  $CENTER\_TIME \leftarrow [ct - \Delta T, ct, ct + \Delta T]$
  for $CenterTime$ in $CENTER\_TIME$ **do**
    Get DAS data from $ct - T/2$ to $ct + T/2$
    Find the pos closest to $event.CrossPos$ in $CenterPos$
    Get sample data by slicing DAS data from $pos - \Delta D$ to $pos + \Delta D$
    Perform Z-score normalization on the sample data channel-wise along the time dimension
    Save the sample data in PNG format
  end for
end for

2) Details of DAShip establishment: The method for constructing the DAShip is detailed in algorithm 2, resulting in

a total sample count of 55875. The details of the DAShip establishment are shown in Fig. 13. In the establishment process, the CrossTime and CrossPos of a ship passage event from the clean AIS records are first used to pinpoint the ship wake in the DAS data, generating a ship sample with a 1-minute time duration and a 1-km spatial range. Then, a fixed time-shifting method is introduced to enhance this ship sample with a 0.2-minute time shift. Moreover, the corresponding ship speed and ship length are used to calculate the intrinsic passage time, thereby leveraging the proposed adaptive annotation method for determining the annotation box size. Finally, based on the corresponding features such as ship speed, ship angle, heading, and ship type, the label for this ship wake annotation can be generated.

The annotation accuracy of the DAShip is mainly influenced by the quality of AIS records, especially for low-speed ships. As aforementioned, low-speed ships have longer AIS-reporting time intervals, and their signals are easily overwhelmed by ocean waves, making them difficult for experts to discern. Although the AIS-based ship passage cleaning and the adaptive annotation method are proposed to reduce annotation errors for low-speed ship passages, the quality of low-speed ship passage annotation cannot be compared to that of high-speed ship passage annotation.

D. Establishing Waveset

Subsequently, according to the time of AIS-based ship passage events, the time range devoid of ship passage events can be derived, which can be used to obtain the wave samples from massive DAS data, including a total of 158505 images. The corresponding wave dataset (Waveset) can be established as algorithm 3, for enhancing the generalization of the online ship detector.

Algorithm 3 Establishing Waveset

$\Delta T \leftarrow 5\ minutes$
$\Delta D \leftarrow 0.5\ km$
$T \leftarrow 1\ minute$
$CenterPos \leftarrow [5, 5.5, 6, ..., 12] km$
$\mathbf{E} \leftarrow$ AIS-based ship passage events
Sort $\mathbf{E}$ by $CrossTime$
for i in $0, 1, ..., len(\mathbf{E}) - 1$ **do**
  $ct0 \leftarrow \mathbf{E}[i].CrossTime$
  $ct1 \leftarrow \mathbf{E}[i+1].CrossTime$
  if $ct1 - ct0 > \Delta T$ **then**
    $CENTER\_TIME \leftarrow (ct0 + ct1)/2$
    Get DAS data from $CENTER\_TIME - T/2$ to $CENTER\_TIME + T/2$
    Find the pos closest to $event.CrossPos$ in $CenterPos$
    Get sample data by slicing DAS data from $pos - \Delta D$ to $pos + \Delta D$
    Perform Z-score normalization on the sample data channel-wise along the time dimension
    Save the sample data in PNG format
  end if
end for

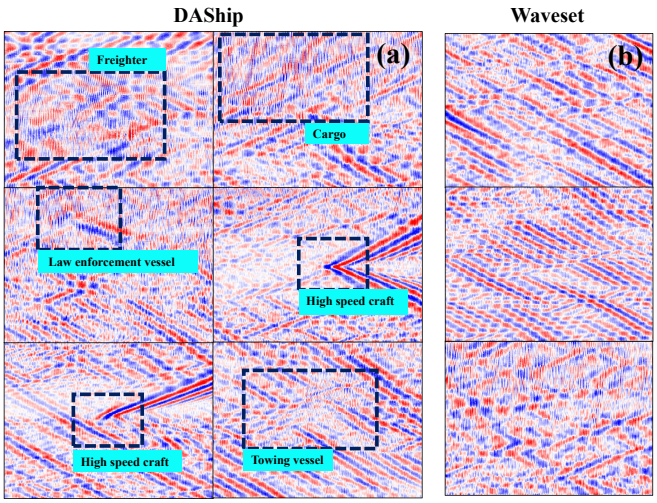

Fig. 14. Details of the proposed datasets: (a) Samples of annotated images in DAShip; (b) Samples in Waveset.

The details of DASship and Waveset are shown in Fig. 14. For the high-speed crafts, the produced ship wake is pronounced and the time dimension and spatial dimension of its peak represent the ship passage event's time and position, according to the analysis in Fig.3. In the proposed annotation method, the peak of the ship wake is in the center of the annotation box, and the predicted center of box can be used to derive the ship passage event's time and position. For the slow-speed ships, such as cargos, freighters, and towing vessels, a larger annotation box is employed to encompass as much of the ship-induced disturbance as possible, through the proposed adaptive annotation method.

To the best of our knowledge, the proposed DASship is the first DAS-based ship annotation dataset, so Table III provides the comparison of other optical remote sensing ship detection datasets. The DAShip and Waveset are available in https://www.alipan.com/s/sTdL3zSRiPo.

E. Online ship detection and identification framework

To evaluate the DAShip and Waveset in ship detection application, an online ship detection and identification framework is proposed, as illustrated in Fig. 15 and Fig. 16, consisting of:

(1) Model-based ship passage detection: Firstly, the incoming raw DAS data flow is segmented according to the size of sample size (1-km spatail range and 1-minute time range). The segmented images are then processed by the ship detector trained on the DAShip and Waveset. The detector utilizes object detection models such as YOLO or Faster-RCNN. The center of the detected annotation box serves as the the location of ship passage within the image sample, while the confidence of the detection is used to mitigate false positives.

(2) Calculating ship event information from samples: Since the raw DAS data flow is segmented according to the pre-known position centroids and timestamps, each image sample is associated with specific geolocation and timestamp information. Consequently, the center of annotation box in

TABLE III
COMPARISON OF OPTICAL REMOTE SENSING SHIP DETECTION DATASETS.

Dataset	Image source	#Images	Image Size	#Ship Categories	#Ship instances	Spatial resolution	Year
DOTA [5]	Multi sources	2806	800∼4000	15	188,282	-	2018
SeaShips [7]	Camera	31455	1920×1080	6	40,077	-	2018
HRSID [3]	Google Earth and Baidu Map	21,761	-	13	55,740	0.15-1.2m	2019
MASATI [37]	Microsoft Bing maps	6,212	512×512	1	3,313	-	2019
FGSD [38]	Google Earth	2,612	930×930	43	5,634	0.12-1.93m	2020
ShipRSImageNet [39]	Multi sources	3,435	930×930 ∼1.4k×1k	50	17,573	0.12-6m	2020
SWIM [8]	Visible waveband satellite; aerial images	14,610	768×768	1	15,356	0.5-2.5m	2021
DAShip	iDAS	55,875	1860×1386	10	18,625	4m	

image samples can be converted into actual passage time and geographic location, defined as the predicted CrossTime and CrossPos. The calculation results with a confidence less than $conf_{thres}$ are discarded and thus the sample-based ship passage events are obtained.

Algorithm 4 Overlapped ship detection method

Input DAS data flow from t to $t+1$ minute
$CenterTime \leftarrow [t-0.3, t-0.1, t+0.1, t+0.3, t+0.5]$
$CenterPos \leftarrow [5, 5.5, 6, ..., 12]km$
for cp in $CenterPos$ **do**
  for ct in $CenterTime$ **do**
    Get $sample_{ct,cp}$ from DAS with time range[$ct-0.5, ct+0.5$] and position range[$cp-0.5, cp+0.5$]
    $dect_{ct,cp} \leftarrow$ Detector ($sample_{ct,cp}$)
    if $dect_{ct,cp}.conf > 0.5$ **then**
      $\mathbf{E} \leftarrow (dect_{ct,cp}.(CrossTime, CrossPos, conf))$
    end if
  end for
end for
Sort $\mathbf{E}$ in descending order of $conf$
repeat
  $CT, CP =$$\mathbf{E}$[0].$(CrossTime, CrossPos)$
  for i in 0 to len($\mathbf{E}$) **do**
    if $\mathbf{E}[i].CrossTime$ in $(CT - err\_time, CT + err\_time)$ **then**
      if $\mathbf{E}[i].CrossPos$ in $(CP - err\_pos, CP + err\_pos)$ **then**
        $e \leftarrow \mathbf{E}[i]$
      end if
    end if
  end for
  if $len(e) \geq NUMS$ **then**
    $ShipEvents \leftarrow (CT, CP)$
  end if
  Remove e from $\mathbf{E}$
until $\mathbf{E}$ is empty
return $ShipEvents$

(3) Overlapped ship detection: Given the temporal and spatial overlaps inherent in sample generation, the same ship passage event may be captured in multiple distinct detection outcomes. Hence an overlapped ship detection method, aas outlined in algorithm 4, is proposed to fuse multiple detection results into a single detection result. By integrating ship passage information detected across various image samples, the precision of ship detection can be significantly improved.

(4) Comparing the detection results with AIS-based ship passage events to obtain DAS-based ship detection coverage and dark ship events. Specifically, the DAS-predicted and AIS-based ship passages are compared according to the DAS-based and AIS-based ship events comparison in Fig.15. To further discuss the comparion result of the DAS-predicted and AIS-based ship passages, a metric as a joint detection ratio is defined in this paper. The joint detection ratio of AIS-based ship passages is calculated as follows:

$$\frac{Num(AIS\ ships \rightarrow DAS\ ships)}{Num(AIS\ ships)} \tag{1}$$

The joint detection ratio of DAS-basd ship passages is calculated as follows:

$$\frac{Num(DAS\ ships \rightarrow AIS\ ships)}{Num(DAS\ ships)} \tag{2}$$

where the notation $DAS\ ships \rightarrow AIS\ ships$ means matching the DAS-based ships with the AIS-based ships by using the predicted CrossTime and CrossPos. Given the ship passage of CrossTime and CrossPos, if exists an AIS-based ship with Time and Position satisfying that $Time - ErrTime \leq CrossTime \leq Time + ErrTime$ and $Position - ErrPosition \leq CrossPos \leq Position + ErrPosition$, the DAS-based ship is considered a match to the AIS-based ship. The reason calculating the respective joint detection ratio for DAS-based and AIS-based ships is the inherent presence of estimation errors and potential loss of ship passage events in both DAS-based and AIS-based systems. Specifically, the AIS-based ship passage is calculated under the assumption that the ship undergos the uniform acceleration, resulting in the estimated error in ship Crosspos and CrossTime. Meanwhile, DAS-based ship detection using object detection models may experience performance drawbacks. Thus, it is necessary to compare DAS-based and AIS-based ships with each other according to the joint detection ratio.

(5) Ship identification: Inputting dark ship detection results into the ship feature classifiers trained on DAShip, analyzing ship speed, heading, angle range, and ship type.

The real-time capability for ship detection is also a key aspect. According to $CenterTime$ and $CenterPos$ in algorithm 4, this frame rate of the detector should be at least

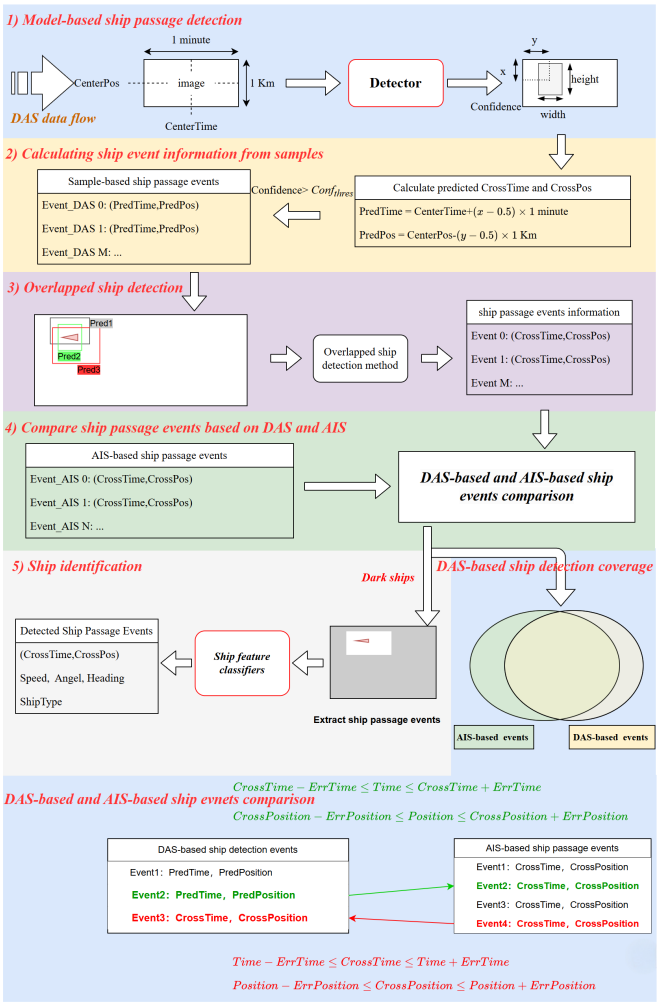

Fig. 15. online ship detection and identification framework.

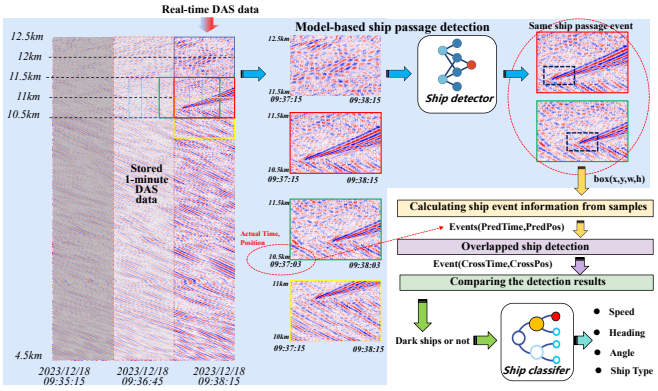

Fig. 16. Framework workflow.

$5 \times 15/60 = 1.25 frame/second$ to accommodate new DAS data incoming every minute. Consequently, the computational requirements of this framework are light. To enhance the real-time capability, the interval for generating DAS data can be reduced to 1 second, thereby increasing the detector's inference frame rate to 75 $frames/second$, a rate that is readily attainable.

TABLE IV
SHIP DETECTOR PERFORMANCE.

Model	Precision	Recall	mAP50	mAP50-95	F1 Score
YOLOv8s	0.896	0.864	0.923	0.872	0.880
YOLOv8l	0.912	0.868	0.931	0.886	0.889
YOLOv5s	0.898	0.859	0.923	0.862	0.878
YOLOv5l	0.916	0.862	0.931	0.876	0.888
Faster R-CNN (ResNet-50-FPN)	0.520	0.875	0.803	0.420	0.652
Faster R-CNN (Vgg-16-FPN)	0.505	0.861	0.785	0.430	0.637

V. EXPERIMENT AND DISCUSSION

The proposed DAShip provides the annotation of ship passage event and its corresponding ship speed, ship cross-angle, ship heading, and ship type. In this experiment, the proposed DAShip and Waveset are firstly evaluated for the ship detection and the coarse ship identification by leveraging the object detection models such as YOLO and Faster R-CNN. Moreover, an ablation study is conducted to evaluate the adaptive annotation method. Subsequently, the proposed ship detection framework is applied to achieve the dark ship detection. Furthermore, the joint detection ratio is introduced to analyze the ship dectection coverage between DAS and AIS data.

Utilizing the proposed datasets DAShip and Waveset, YOLOv5 [40], YOLOv8 [41], and Faster R-CNN models are employed to detect ship passage events, as well as to determine ship speed, angle, and heading. The DAShip is divided temporally according to a ratio of 8:1:1 for training, validation, and testing, respectively. The training set, comprising 44698 samples, covers the time period from 2023/11/14 13:55:32 to 2024-03-08 21:10:12. The validation set, consisting of 5589 samples, ranges from 2024-03-08 21:10:12 to 2024-03-18 20:44:50. The testing set, also comprising 5589 samples, ranges from 2024-03-18 20:44:50 to 2024/03/27 01:01:30. Similarly, the Waveset samples are also divided and randomly selected into training(18720 samples), validation (2340 samples), and test (2340 samples) sets in the aforementioned time range that the DAShip are based on.

A. Ship detection

YOLOv5s, YOLOv5l, YOLOv8s, YOLOv8l, Faster R-CNN with ResNet-50, and Faster R-CNN with Vgg16 are trained using the same aforementioned training set, and the performances are shown in Table IV. For example, the details of training process of YOLOv8s are depicted in Fig.17.

The detection of ship passage events is illustrated in Fig.18. These models trained on DAShip and Waveset can successfully identify the passage events of low-speed ships, as shown in Fig.18(c) and (d), addressing the challenge of manual identification due to the lack of significance in DAS data.

In Table IV, these models exhibit similar recall metrics, but the Faster R-CNN models show lower precision. Thus, the Faster R-CNN models are not considered in our proposed ship detection framework due to their inferior performance. YOLOv5l and YOLOv8l have approximately three times the FLOPS compared to YOLOv5s and YOLOv8s. The lower

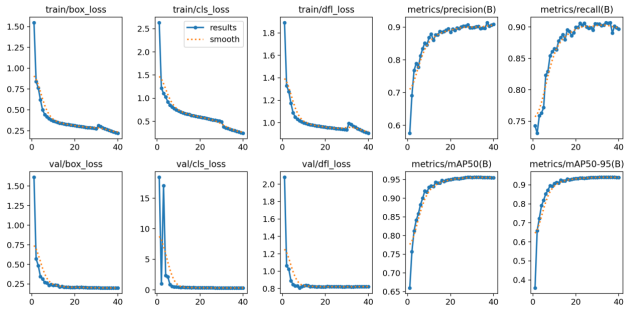

Fig. 17. Training details.

TABLE V
ABLATION EXPERIMENT FOR YOLOV8S.

Experiment	Precision	Recall	mAP50	mAP50-95	F1 Score
NW-A[a]	0.91	0.873	0.95	0.926	0.891
W-0.3[b]	0.892	0.857	0.911	0.859	0.874
W-0.5[c]	0.909	0.857	0.92	0.898	0.882

[a]NW-A:Trained without Waveset and the DAShip is annotated with adaptive annotation box;
[b]W-0.3:Trained with Waveset and the DAShip is annotated with fixed size(0.3) box;
[c]W-0.5:Trained with Waveset and the DAShip is annotated with fixed size(0.5) box;

FLOPS of YOLOv5s and YOLOv8s enable faster online detection of ship passage events. In this experiment, YOLOv8s demonstrates superior recall compared to YOLOv5s, aiding in the reduction of false positive detections in extensive DAS data. Therefore, the YOLOv8s model is chosen as the detector in the online ship detection framework for dark ship detection.

To validate the effectiveness of the adaptive annotation method, a fixed-size annotation method (fixed width and height of annotation box) is introduced in DAShip. YOLOv8s is trained using the same data samples in Table IV. Table V displays the performance of YOLOv8s with fixed sizes of 0.3 and 0.5, highlighting that the adaptive annotation method achieves a higher recall rate compared to the fixed-size annotation method.

To investigate whether the introduction of Waveset helps reduce the false positive rate of ship passage events, an experiment is conducted using exclusively DAShip samples to train YOLOv8s(NW-A), as shown in the Table V. YOLOv8s (NW-A) outperforms than YOLOv8s in Table IV across all metrics. Nevertheless, in the subsequent ship coverage experiment, the performance of the YOLOv8s (NW-A) model is not as good as that of YOLOv8s.

B. Ship identification

Using the same dataset partitioning schemes, YOLOv5s, YOLOv5l, YOLOv8s, YOLOv8l, and Faster R-CNN models are trained for coarse-grained ship identification. The performances are detailed in Table VI. Clearly, the YOLO models outperform the Faster R-CNN models in terms of the recall, mAP50, and mAP50-95 metrics. As aforementioned, the ship speed and ship corss-angle significantly impact the pattern of the DAS-sensed ship wake, while ship heading and type are theoretically more challenging to classify. Therefore, the classification of ship heading and type is further discussed as follows.

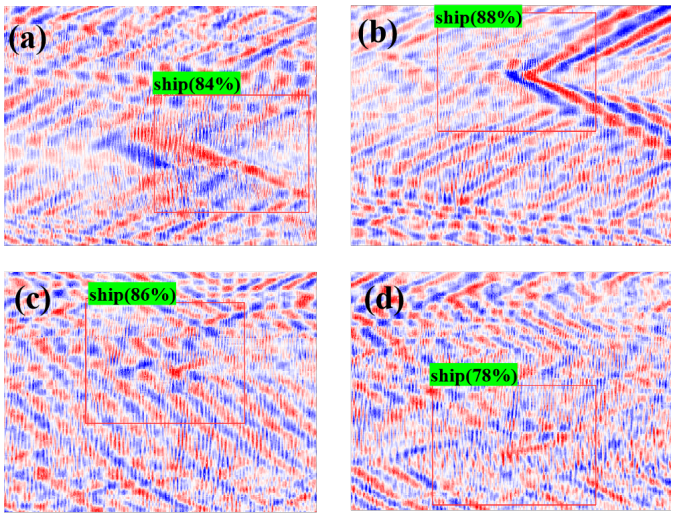

Fig. 18. Ship detection examples. AIS records: (a) The ship passed at a speed of 7.17m/s at 16:00:58 2024/3/26; (b) The ship passed at a speed of 14.18m/s at 16:02:30 2024/3/26; (c) The ship passed at a speed of 4.94m/s at 16:50:41 2024/3/26; (d) The ship passed at a speed of 3.68m/s at 16:52:21 2024/3/26.

TABLE VI
COARSE-GRAINED SHIP IDENTIFICATION PERFORMANCE.

Model	Task	Class	Precision	Recall	mAP50	mAP50-95	F1 Score
YOLOv8s	Speed	High-speed	0.832	0.93	0.935	0.914	0.878
		Low-speed	0.905	0.836	0.931	0.865	0.869
	Heading	S→N	0.806	0.805	0.875	0.83	0.805
		N→S	0.872	0.771	0.877	0.831	0.818
	Angle	>90°	0.834	0.79	0.869	0.823	0.811
		<=90°	0.852	0.81	0.881	0.833	0.830
YOLOv81	Speed	High-speed	0.816	0.953	0.945	0.924	0.879
		Low-speed	0.91	0.853	0.921	0.875	0.881
	Heading	S→N	0.839	0.821	0.891	0.846	0.830
		N→S	0.882	0.807	0.892	0.848	0.843
	Angle	>90	0.847	0.791	0.877	0.837	0.818
		<=90°	0.872	0.807	0.893	0.846	0.838
YOLOv5s	Speed	High-speed	0.825	0.939	0.904	0.841	0.878
		Low-speed	0.898	0.838	0.904	0.841	0.867
	Heading	S→N	0.825	0.8	0.881	0.82	0.812
		N→S	0.862	0.792	0.883	0.817	0.826
	Angle	>90°	0.822	0.784	0.871	0.813	0.803
		<=90°	0.856	0.798	0.885	0.819	0.826
YOLOv51	Speed	High-speed	0.82	0.928	0.908	0.877	0.871
		Low-speed	0.899	0.851	0.92	0.865	0.874
	Heading	S→N	0.854	0.822	0.897	0.846	0.838
		N→S	0.88	0.815	0.896	0.844	0.846
	Angle	>90°	0.824	0.803	0.874	0.826	0.813
		<=90°	0.881	0.803	0.892	0.839	0.840
Faster RCNN (ResNet-50-FPN)	Speed	High-speed	0.846	0.660	0.819	0.337	0.74
		Low-speed	0.781	0.735	0.727	0.342	0.76
	Heading	S→N	0.792	0.442	0.644	0.360	0.57
		N→S	0.811	0.500	0.670	0.544	0.620
	Angle	>90°	0.836	0.580	0.720	0.338	0.68
		<=90°	0.805	0.604	0.711	0.342	0.69
Faster RCNN (Vgg-16-FPN)	Speed	High-speed	0.830	0.534	0.798	0.348	0.65
		Low-speed	0.755	0.739	0.686	0.362	0.75
	Heading	S→N	0.774	0.467	0.642	0.357	0.58
		N→S	0.788	0.513	0.673	0.561	0.62
	Angle	>90°	0.871	0.538	0.717	0.339	0.67
		<=90°	0.825	0.548	0.686	0.302	0.66

1) Heading detection: DAS technology measures one-dimensional vibration signals on the optical fiber by converting the fiber into a linear array of vibration sensors. Therefore, it is inherently unable to distinguish which side of the fiber the vibration source is located on, leading to directional ambiguity [12], [42].

Consider two identical ships moving at the same speed and angle, crossing the fiber cable symmetrically at the same

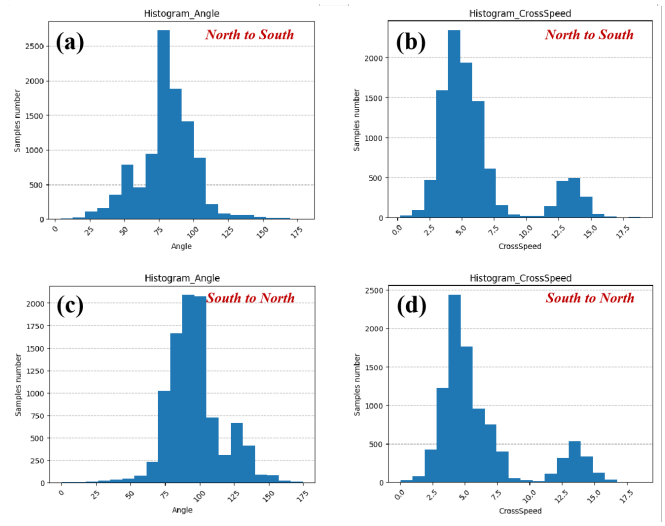

Fig. 19. The speed and angle distribution of ship passage events under different headings are as follows: (a) and (b) represent the speed and angle distribution of ships traveling from north to south; (c) and (d) represent the speed and angle distribution of ships traveling from south to north.

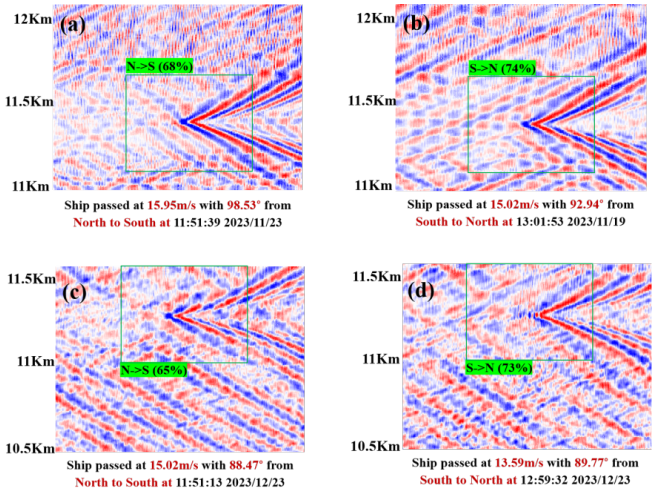

Fig. 20. Heading detection.

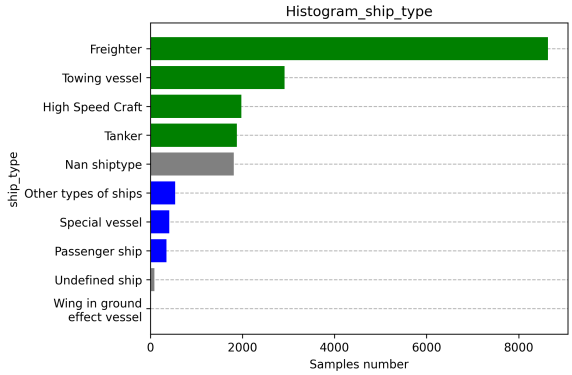

Fig. 21. ShipType distribution.

time. Despite their similarities, due to variations in hydrological conditions (such as water flow direction and geological features) on either side of the submarine optical fiber cable, the vibration signals produced by the two ships will exhibit distinct characteristics. These differences are typically difficult to discern with traditional algorithms but can be effectively captured and analyzed by deep learning models trained on extensive ship passage data.

Leveraging the DAShip, a YOLOv8s model is trained to classify ship passage heading as North to South ($N \rightarrow S$) and South to North ($S \rightarrow N$). The performance of the model is presented in Table VI. It is evident that the ship heading can be classified by the trained model, thus employing artificial intelligence techniques can address the directional ambiguity issue in submarine cable vibration sensing in this paper.

As aforementioned, the patterns of ship passage samples are primarily determined by the angles and speeds of ship passages. When these patterns vary due to differences in angle or speed distributions across various headings, the model may focus on learning these variations in angle or speed distributions rather than the pattern differences attributable to hydrological conditions. In Fig.19, it is evident that despite different headings, the speed distributions of ship passages are similar, while there are certain differences in angle distributions.

To mitigate the impact of angle distribution differences on the model performance, this experiment focuses on ship samples with angles ranging from 80° to 100°. Within this angle range, samples with different headings exhibit remarkably similar patterns, making them theoretically difficult to distinguish. Fig.20 presents two examples of ship passage detections. In Fig.20(a) and (b), the ship passage events are located at 11.3 km of the optical cable, displaying negligible differences in ship speed and angle but opposite headings. Similarly, Fig.20(c) and (d) depict another example. These examples demonstrate the effectiveness of the trained model in accurately recognizing ship passage headings, even when patterns are highly similar and challenging for experts to distinguish.

2) ShipType classification: The DAShip includes 10 types of ship, including freighter, towing vessel, high speed craft, tanker, Nan shiptype (no ship type reported in AIS), other types of ships, special vessel, passenger ship, wing in ground effect vessel, and undefined ship. The distribution of these ship types is shown in Fig. 21. In this ship type classification experiment, samples labeled as Nan shiptype and undefined ship are excluded, and the samples with the predominant types (92.14% of all samples), such as towing ships, high-speed craft, freighters, and tankers, are used to train a YOLOv8s model. The confusion matrix and precision-recall curve are shown in Fig. 22 and Fig. 23, respectively. Consequently, utilizing the proposed DAShip, the YOLO model demonstrates competitive performance in classifying six ship types. To the best of our knowledge, this is the first model-based approach to ship type detection in DAS data processing.

3) Comparative analysis: Based on the propose adaptive annotation method, the annotation boxes occupy a size proportion of the image samples ranging from 0.3^2 to 0.8^2. Consequently, the ship detection task conducted in this paper is targeted at detecting larger objects.

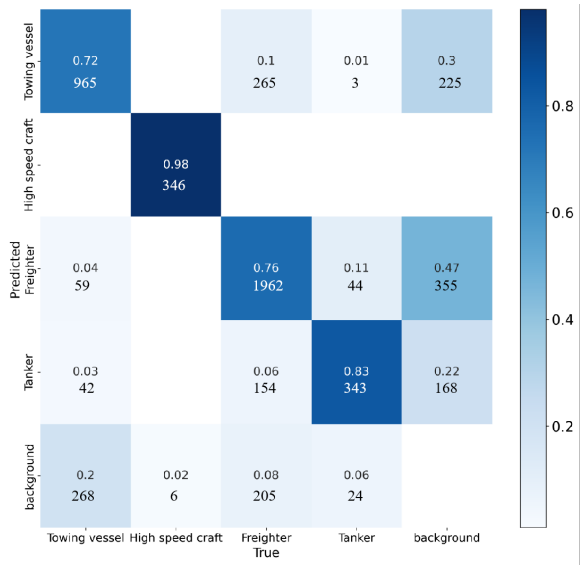

Fig. 22. ShipType confusion matrix.

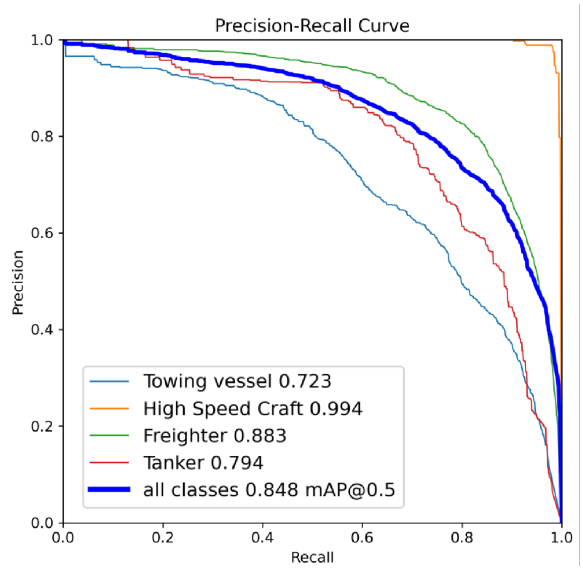

Fig. 23. ShipType PR curve.

YOLO typically exhibits better performance than Faster R-CNN, which can be attributed to its approach of dividing the image into grids and making predictions directly at the grid level, thereby more effectively utilizing global information. For large-sized targets, this method can more efficiently capture the overall structure of the objects. In contrast, Faster R-CNN first generates candidate regions using a Region Proposal Network (RPN) and then performs classification and bounding box regression within these regions. The classifier only receives local information of the ship's wake. In cases of slower-moving vessels, where the wake signal is more likely to be obscured by waves and the annotation boxes are larger, Faster R-CNN's lack of a global perspective can lead to missed detections of such weak wake signals.

Furthermore, YOLO employs an end-to-end training approach, which allows for direct optimization of detection performance. In contrast, Faster R-CNN requires separate training of the RPN and Fast R-CNN stages, making it structurally complex and more challenging to train and tune.

Lastly, the YOLO algorithm is based on single-shot detection, enabling it to predict multiple bounding boxes and category probabilities in a single forward pass. This feature allows YOLO to maintain high processing speed when dealing with large-sized images, making it more suitable for real-time detection and, consequently, for the proposed ship detection framework.

C. Evaluating the proposed framework

In this experiment, the proposed online ship detection and identification framework shown in Fig. 15 is used to assess the DAS-based ship detection coverage with the DAS data flow from 2024/3/19 00:00:00 to 2024/3/27 01:00:00, because this data flow is never used in the model training and testing processes.

1) Ship detection coverage: Leveraging the trained detector (YOLOv8s in Table IV achieving 0.896 precision, 0.864 recall, 0.923 mAP50, 0.872 mAP50-90, and 0.88 F1 score) to process each minute of DAS data, the ship detection coverage can be evaluated. Specifically, $Conf_{thres}$ is 0.5 in the framework shown in Fig.15. In the DAS-based and AIS-based ship events comparison within the proposed framework, the allowable error in time ($ErrTime$) and position ($ErrPosition$) are set at 30 seconds and 0.2 km, respectively. As aforementioned, during the DAShip establishment, the AIS-based ship records were filtered to exclude the slow-moving and problematic ship trajectories, while in the DAS-based and AIS-based ship detection comparison, more lenient filtered constraints on $Error\_speed$ and the time interval(ΔT) shown in Table II are required because these ship trajectories could probably exist.

In this coverage experiment, 2083 AIS-based ship records are obtained, with 1533 records found in the DAS-based ship detections, resulting in a joint detection ratio of 73.6%. Similarly, 2450 DAS-based ship detections are obtained, with 1773 detections found in the AIS-based ship records, yielding a joint detection ratio of 72.4%.

The detection process of the proposed ship detection framework, although distinct from typical detection tasks, can still be evaluated using performance metrics such as precision, recall, and F1-score. In this context, AIS-based ship passages are considered as the true ship passages, making the recall metric equivalent to the joint detection ratio for AIS-based records. Concurrently, DAS-based ship passages are regarded as the total prediction outcomes, with the joint detection ratio for DAS-based ship passages serving as the precision metric. Consequently, the F1 score is determined to be 0.73.

To further analyze the performance of ship detection, a stricter restriction ($Error\_speed = 0.05, \Delta T = 0.1\ minute$) is applied to filter the AIS-based ship record, aiming to obtain more authentic ship trajectories. Consequently, the joint detection ratio of the filtered AIS-based ship records (234 records) reaches 90.17%, indicating that the YOLOv8s detector trained on the DAShip and Waveset can detect most of authentic ship passage events, and there still remains potential for enhancing

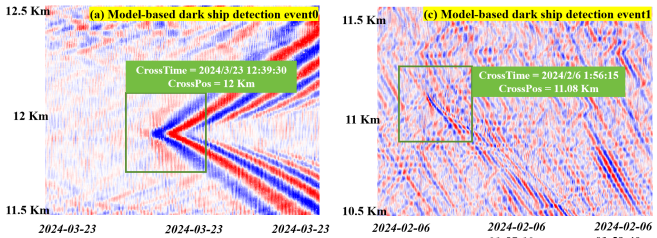

(b) AIS-based ship passage events around 2024/3/23 12:39

CrossTime	CrossPos(Km)	Speed(m/s)	Angle(°)
2024/3/23 12:38:48	11.97	5.15	55.95
2024/3/23 12:49:23	9.18	3.53	155.66

(d) AIS-based ship passage events around 2024/2/6 1:56

CrossTime	CrossPos(Km)	Speed(m/s)	Angle(°)
2024/2/6 1:51:00	11.59	3.67	81.05
2024/2/6 1:59:12	11.83	6.22	69.42

Fig. 24. Model-based Dark Ship Passage Event Detection Results: (a) (c) Samples of Dark ship detection events;(b)(d) AIS Records for Nearby Time Period.

the performance of ship detection.

As aforementioned, the YOLOv8s (NW-A) in Table V outperforms the YOLOv8s in Table IV. However, employing the same filtered constraints, YOLOv8s (NW-A) detects 8396 ship passage events, significantly surpassing the number of AIS-based ship records. 1561 detected ship passage events can be found in AIS-based ship records, yielding a joint detection ratio of 74.93%, while only 1761 AIS-based ship records can be found in the detected ship passage events, resulting in a joint detection ratio of 20.97%. Consequently, YOLOv8s trained without Waveset samples will cause a higher false positive rate, and the Waveset is necessary to train the YOLO model within the online ship detection framework.

2) Dark ship detection: The model-based ship detection method can identify ship passage events that are not reported in AIS information, as depicted in Fig.24. Fig.24(a) illustrates a ship passage event detected by the model at 11.08 km of the optical fiber cable at 1:56:15 on February 26, 2024. Fig.24(b) displays the ship's AIS records in the nearby time period, revealing that the ship passage event detected by the model does not align with any ship passage records in the AIS data. Therefore, utilizing DAS for ship passage event detection can effectively detect dark ship passage events.

D. Discussion

The DAShip sample is collected from the straight submarine cable, so the route of the cable wiil influence the pattern of the ship wake signals sensed by the DAS device. Besides, the coupling of the cables with the submarine sediments affectes the ship wake signal intensity although the Z-score normalization on the sample data channel-wise along the time dimension was applied in the DAShip establishment as shown in algorithm2. Additionally, in other sea regions, the different water depth also affectes the pattern of the ship wakes. Therefore, it is required to continuously collect DAS-based samples from a wide range of marine environments. A more extensive and higher-quality version of the DAShip dataset is still needed. By incorporating diverse marine regions into the dataset, the deep learning models will be exposed to a variety of conditions, such as different sea states, noise levels, and interference patterns, which will ultimately lead to more robust and accurate detection and classification performance.

In real-world maritime environments, the DAS devices are required to be deployed at the communication equipment room and connected to the existing telecommunication optical fiber cables to collect vibration signals [43]. Due to the massive data volume generated, a large storage device such as NAS (Network Attached Storage) is required, while the newly incoming DAS data can be immediately sent into the proposed system to achieve the model-based ship detection and the ship feature classification. Thus, the deployment of overall system is relatively straightforward.

Although the proposed framework has been used to detect dark ships successfully, there is still room for improvement. Firstly, this framework used the common YOLOv8s as the detector and classifier, while a specialized ship detector should be designed to further enchance the detection performance. Secondly, the robustness of the proposed framework is required to enhance, thus it is essential to improve the generalization capabilities of both the ship detector and the ship classifier, which mainly depends on the generalization of the DAShip. Finally, integrating this DAS-based ship detection method with other existing remote sensing methods such as SAR and satellite imaging to achieve more accurate vessel identification warrants further in-depth research.

VI. Conclusion

This paper mainly proposes a large-scale annotated dataset for ship detection (DAShip) and an online ship detection and identification framework for the detection and analysis of dark ships. DAShip is the first ship passage event dataset based on DAS data, which contains 55875 images with 18625 ship instances. Utilizing DAShip, YOLO models are trained and employed in the proposed framework to detect dark ships and analyze ship features, including speed, angle, heading, and ship type from the online DAS data flow. The joint detection ratio of AIS-based and DAS-based ship detection are 73.6% and 72.4%, respectively. Using DAShip, the directional ambiguity of ship passage can be solved, highlighting the superiority of model-based detection over traditional signal processing techniques. Furthermore, with the rich ship feature labels provided by DAShip, the speed, angle, heading, and ship-type classifiers can be developed to achieve competitive performance.

Acknowledgments

This work was supported by (1) National Key R&D Program of China under Grant 2020YFB1806401; (2) in part by the National Natural Science Foundation of China under Grant U2001601,U22A2087; (3) in part by Project supported by Southern Marine Science and Engineering Guangdong Laboratory(Zhuhai) (SML2023SP231); (4) The Program of Marine Economy Development Special Fund (Six Marine Industries) under Department of Natural Resources of Guangdong Province (Project No. GDNRC [2024]17); (5) The Program of Marine Economy Development Special Fund (Six Marine Industries) under Department of Natural Resources of Guangdong Province (Project No. GDNRC [2024]16); (6) GuangDong Basic and Applied Basic Research Foundation under Grant 2022A1515110006.

REFERENCES

[1] H. Wu, Z. Huang, Q. Hu, X. Ran and Q. Mei, "AIS Data-Guided Geolocation Correction Method for Low-Orbit Satellite Remote Sensing Imagery," *IEEE Journal of Selected Topics in Applied Earth Observations and Remote Sensing*, pp.1-25, 2024.

[2] P. Heiselberg, H. B. Pedersen, K. A. Sørensen, and H. Heiselberg, "Identification of Ships in Satellite Images," *IEEE Journal of Selected Topics in Applied Earth Observations and Remote Sensing*, vol. 17, pp. 6045-6054, 2024.

[3] S. Wei, X. Zeng, Q. Qu, M. Wang, H. Su, and J. Shi, "HRSID: A High-Resolution SAR Images Dataset for Ship Detection and Instance Segmentation," *IEEE Access*, vol. 8, pp. 120234-120254, 2020.

[4] Z. Liu, W. Zhang, H. Yu, S. Zhou, W. Qi, Y. Guo, et al., "Improved YOLOv5s for Small Ship Detection With Optical Remote Sensing Images," *IEEE Geoscience and Remote Sensing Letters*, vol. 20, pp. 1-5, 2023.

[5] G.-S. Xia, X. Bai, J. Ding, Z. Zhu, S. Belongie, J. Luo, et al., "DOTA: A large-scale dataset for object detection in aerial images," in *Proceedings of the IEEE conference on computer vision and pattern recognition*, 2018, pp. 3974-3983.

[6] Y. Zhang, Y. Yuan, Y. Feng, and X. Lu, "Hierarchical and robust convolutional neural network for very high-resolution remote sensing object detection," *IEEE Transactions on Geoscience and Remote Sensing*, vol. 57, pp. 5535-5548, 2019.

[7] Z. Shao, W. Wu, Z. Wang, W. Du, and C. Li, "SeaShips: A Large-Scale Precisely Annotated Dataset for Ship Detection," *IEEE Transactions on Multimedia*, vol. 20, pp. 2593-2604, 2018.

[8] F. Xue, W. Jin, S. Qiu, and J. Yang, "Rethinking Automatic Ship Wake Detection: State-of-the-Art CNN-Based Wake Detection via Optical Images," *IEEE Transactions on Geoscience and Remote Sensing*, vol. 60, pp. 1-22, 2022.

[9] Z. Wang, G. Hou, Z. Xin, G. Liao, P. Huang, and Y. Tai, "Detection of SAR Image Multiscale Ship Targets in Complex Inshore Scenes Based on Improved YOLOv5," *IEEE Journal of Selected Topics in Applied Earth Observations and Remote Sensing*, vol. 17, pp. 5804-5823, 2024.

[10] J. Chen, K. Ai, H. Li, X. Xiao, C. Fan, Z. Yan, et al., "Surface and Underwater Surveillance based on Highly Sensitive Distributed Fiber-optic Hydrophone," *2023 Optical Fiber Communications Conference and Exhibition (OFC)*, pp. 1-3, 2023.

[11] D. Rivet, B. de Cacqueray, A. Sladen, A. Roques, and G. Calbris, "Preliminary assessment of ship detection and trajectory evaluation using distributed acoustic sensing on an optical fiber telecom cable," *The Journal of the Acoustical Society of America*, vol. 149 4, p. 2615, 2021.

[12] M. Landrø, L. Bouffaut, H. J. Kriesell, J. R. Potter, R. A. Rørstadbotnen, K. Taweesintananon, et al., "Sensing whales, storms, ships and earthquakes using an Arctic fibre optic cable," *Scientific Reports*, vol. 12, no. 1, p. 19226, 2021.

[13] Y. Liu, J. Yang, Z. Wang, B. Wu, L. Shuai, L. Ye, et al., "High Performance Miniaturized DAS-based hydrophone (HyDAS) with Spatial Deviation Method for Ship Detection," *28th International Conference on Optical Fiber Sensors*, 2023.

[14] M. Liang, J. Su, R. W. Liu, and J. S. L. Lam, "AISClean: AIS data-driven vessel trajectory reconstruction under uncertain conditions," *Ocean Engineering*, vol. 306, p. 117987, 2024.

[15] Y. Zhou, H. Liu, F. Ma, Z. Pan, and F. Zhang, "A Sidelobe-Aware Small Ship Detection Network for Synthetic Aperture Radar Imagery," *IEEE Transactions on Geoscience and Remote Sensing*, vol. 61, pp. 1-16, 2023.

[16] M. Zhu, G. Hu, H. Zhou, and S. Wang, "Multiscale Ship Detection Method in SAR Images Based on Information Compensation and Feature Enhancement," *IEEE Transactions on Geoscience and Remote Sensing*, vol. 60, pp. 1-13, 2022.

[17] B. Hu and H. Miao, "An Improved Deep Neural Network for Small-Ship Detection in SAR Imagery," *IEEE Journal of Selected Topics in Applied Earth Observations and Remote Sensing*, vol. 17, pp. 2596-2609, 2024.

[18] K. m. Kang and D. j. Kim, "Ship Velocity Estimation From Ship Wakes Detected Using Convolutional Neural Networks," *IEEE Journal of Selected Topics in Applied Earth Observations and Remote Sensing*, vol. 12, pp. 4379-4388, 2019.

[19] S. K. Joshi, S. V. Baumgartner, and B. Tings, "Efficient Size and Heading Angle Estimation of Ships in SAR and ISAR Images," *IEEE Geoscience and Remote Sensing Letters*, vol. 21, pp. 1-5, 2024.

[20] Zhao, Tianjie et al. "Artificial intelligence for geoscience: Progress, challenges, and perspectives." *Innovation (Camb)*vol. 5,5 100691, 2024.

[21] J. Zhang, W. Sheng, H. Zhu, S. Guo, and Y. Han, "MLBR-YOLOX: An Efficient SAR Ship Detection Network With Multilevel Background Removing Modules," *IEEE Journal of Selected Topics in Applied Earth Observations and Remote Sensing*, vol. 16, pp. 5331-5343, 2023.

[22] C. Tian, D. Liu, F. Xue, Z. Lv, and X. Wu, "Faster and Lighter: A Novel Ship Detector for SAR Images," *IEEE Geoscience and Remote Sensing Letters*, vol. 21, pp. 1-5, 2024.

[23] Tan, Xiangdong et al. "YOLO-RC: SAR Ship Detection Guided by Characteristics of Range-Compressed Domain." *IEEE Journal of Selected Topics in Applied Earth Observations and Remote Sensing*, pp 1-18, 2024

[24] Y. Yin, X. Cheng, F. Shi, M. Zhao, G. Li, and S. Chen, "An Enhanced Lightweight Convolutional Neural Network for Ship Detection in Maritime Surveillance System," *IEEE Journal of Selected Topics in Applied Earth Observations and Remote Sensing*, vol. 15, pp. 5811-5825, 2022.

[25] B. Yan, H. Li, K. Zhang, X. Xiao, T. He, C. Fan, et al., "Quantitative Identification and Localization for Pipeline Microleakage by Fiber Distributed Acoustic Sensor," *Journal of Lightwave Technology*, vol. 41, pp. 5460-5467, 2023.

[26] Y. Duan, L. Liang, X. Tong, B. Luo, and B. Cheng, "Application of pipeline leakage detection based on distributed optical fiber acoustic sensor system and convolutional neural network," *Journal of Physics D: Applied Physics*, vol. 57, p. 105102, 2023.

[27] Y.-y. Wang, S.-w. Zhao, C. Wang, H.-b. Zhang, and X.-d. Li, "Intelligent detection and recognition of multi-vibration events based on distributed acoustic sensor and improved YOLOv8 model," *Optical Fiber Technology*, vol. 84, p. 103706, 2024.

[28] T. He, S. Zhang, H. Li, Z. Zeng, J. Chen, Z. Yan, et al., "An Efficient Separation and Identification Algorithm for Mixed Threatening Events Applied in Fiber-Optic Distributed Acoustic Sensor," *IEEE Sensors Journal*, vol. 23, no. 20, pp. 24763-24771, 2023.

[29] N. Wu, T. Xing, and Y. Li, "Multi-Scale Progressive Fusion Attention Network Based on Small Sample Training for DAS Noise Suppression," *IEEE Transactions on Geoscience and Remote Sensing*, vol. 60, pp. 1-12, 2022.

[30] Y. Li, M.-X. Zhang, Y. Zhao, and N. Wu, "Distributed Acoustic Sensing Vertical Seismic Profile Data Denoising Based on Multistage Denoising Network," *IEEE Transactions on Geoscience and Remote Sensing*, vol. 60, pp. 1-17, 2022.

[31] Y. Tian, T. Lin, Y. Li, and N. Wu, "Efficient SPSNet for Downhole Weak DAS Signals Recovery," *IEEE Geoscience and Remote Sensing Letters*, vol. 19, pp. 1-5, 2022.

[32] H. Ma, J. Yu, Y. Wang, N. Wu, and Y. Li, "A Global and Multiscale Denoising Method Based on Generative Adversarial Network for DAS VSP Data," *IEEE Transactions on Geoscience and Remote Sensing*, vol. 61, pp. 1-15, 2023.

[33] J. Li, P. Xiong, Y. Li, and Q. Feng, "DAS Noise Suppression Network Based on Distributing-Local-Attention Expansion," *IEEE Geoscience and Remote Sensing Letters*, vol. 21, pp. 1-5, 2024.

[34] H. Lv, X. Zeng, F. Bao, J. Xie, R. Lin, Z. Song, et al., "ADE-Net: A Deep Neural Network for DAS Earthquake Detection Trained With a Limited Number of Positive Samples," *IEEE Transactions on Geoscience and Remote Sensing*, vol. 60, pp. 1-11, 2022.

[35] R. Min, Y. Chen, H. Wang, and Y. Chen, "DAS Vehicle Signal Extraction Using Machine Learning in Urban Traffic Monitoring," *IEEE Transactions on Geoscience and Remote Sensing*, vol. 62, pp. 1-10, 2024.

[36] L. Thiem, S. Wienecke, K. Taweesintananon, M. Vaupel, and M. Landrø, "Ship noise characterization for marine traffic monitoring using distributed acoustic sensing," *2023 IEEE International Workshop on Metrology for the Sea; Learning to Measure Sea Health Parameters (MetroSea)*, pp. 334-339, 2023.

[37] Gallego A J, Pertusa A, Gil P. "Automatic ship classification from optical aerial images with convolutional neural networks" *Remote Sensing*, vol.10, no.4, pp.511, 2018.

[38] K. Chen, M. Wu, J. Liu, and C. Zhang, "FGSD: A dataset for fine-grained ship detection in high resolution satellite images," CoRR, vol.abs/2003.06832, 2020. [Online]. Available: https://arxiv.org/abs/2003.06832

[39] Zhang, Zhengning et al "ShipRSImageNet: A Large-Scale Fine-Grained Dataset for Ship Detection in High-Resolution Optical Remote Sensing Images." *IEEE Journal of Selected Topics in Applied Earth Observations and Remote Sensing*, vol.14, pp:8458-8472, 2021.

[40] Glenn Jocher, "Ultralytics YOLOv5," https://github.com/ultralytics/yolov5, 2020.

[41] Glenn Jocher and Ayush Chaurasia and Jing Qiu, "Ultralytics YOLOv8," https://github.com/ultralytics/ultralytics, 2023.

[42] J. P. Verdon, S. A. Horne, A. Clarke, A. L. Stork, A. F. Baird, and J. M. Kendall, "Microseismic monitoring using a fibre-optic Distributed Acoustic Sensor (DAS) array," *Geophysics*, vol. 85, no. 3, p.0-11, 2020.
[43] Chen, S., Liu, K., Han, J., Sui, Q., Li, Z. "Photonic Integrated Sensing and Communication System Harnessing Submarine Fiber Optic Cables for Coastal Event Monitoring." *IEEE Communications Magazine*, vol.60, pp.110-116,2022.

Wenjin Huang received the BE degree in automation and the ME degree in circuits and system from Sun Yat-Sen University, Guangzhou, China in 2012 and 2015, respectively, and the PhD degree from Sun Yat-Sen University, Guangzhou, China in 2021. He is currently pursuing postdoctoral research at Sun Yat-Sen University, Guangzhou, China, and his research interests include machine learning and high performance computing.

Shaoyi Chen is a Ph.D. student in the School of Electronics and Information Technology at Sun Yat-sen University. He received his B.S. degree from Beijing Normal University, China, in 2008, and his M.Sc. degree from Beihang University, Beijing, China, in 2011. His research interests include distributed fiber sensing systems and signal processing based on optical fiber devices.

Yichang Wu received the Ph.D. degree from Sun Yat-sen University in 2024. He is currently a postdoctoral fellow with the Hong Kong Polytechnic University. His research interests include optical fiber sensors, digital signal processing, and machine learning.

Ruihua Li received her B.E. degree in Communication Engineering and M.S. degree in Information and Communication Engineering from Sun Yat-Sen University Electronics and Information Technology in 2019 and 2023, respectively. Her research interests include signal processing and data analysis on distributed optical fiber sensors.

TianruiLi received the B.E. degree in electronic information science and technology in 2017 and M.E degree Circuit and System in 2022 from Sun Yat-Sen University, Guangzhou, China. He is currently pursuing a doctoral degree in the School of Electronics and Information Technology at the same university. His research interests include FPGA-based cryptography accelerators and sensing systems.

Yihua Huang received the BE degree in mechanical engineering from Nanjing University of Science and Technology, Nanjing, China in 1996, the ME degree in aerospace propulsion engineering from Nanjing University of Science and Technology, Nanjing, China in 1999, and the PhD degree from University of Science and Technology of China, Hefei, China in 2002. From 2002 to 2013, he has been an assistant and associate professor at Department of Electronic and Communication Engineering, Sun Yat-Sen University, Guangzhou, China. From 2013, he has been an professor at School of Electronics and Information Technology, Sun Yat-Sen University, Guangzhou, China. His research interests include deep neural network acceleration on FPGA and system design on FPGA.

Xiaochun Cao is a Professor of School of Cyber Science and Technology, Shenzhen Campus, Sun Yat-sen University. He received the B.E. and M.E. degrees both in computer science from Beihang University (BUAA), China, and the Ph.D. degree in computer science from the University of Central Florida, USA, with his dissertation nominated for the university level Outstanding Dissertation Award. After graduation, he spent about three years at ObjectVideo Inc. as a Research Scientist. From 2008 to 2012, he was a professor at Tianjin University. Before joining SYSU, he was a professor at Institute of Information Engineering, Chinese Academy of Sciences. He has authored and coauthored over 200 journal and conference papers. In 2004 and 2010, he was the recipients of the Piero Zamperoni best student paper award at the International Conference on Pattern Recognition. He is on the editorial boards of IEEE Trans. on Image Processing and IEEE Trans. on Multimedia, and was on the editorial board of IEEE Trans. on Circuits and Systems for Video Technology.

Zhaohui Li is a professor in the School of Electronics and Information Technology at Sun Yat-sen University. He obtained his B.S. from the Department of Physics and his M.Sc. from the Institute of Modern Optics of Nankai University in 1999 and 2002, respectively, and received his Ph.D. from Nanyang Technological University in 2007. His research interests include optical communication systems, optical signal processing technology, and ultra-fine measurement systems